Two-cluster solutions in an ensemble of generic limit-cycle oscillators with periodic self-forcing via the mean-field

Lennart Schmidt[1,2] and Katharina Krischer[1,*]

[1] *Physik-Department, Nonequilibrium Chemical Physics, Technische Universität München, James-Franck-Str. 1, D-85748 Garching, Germany*

[2] *Institute for Advanced Study - Technische Universität München, Lichtenbergstr. 2a, D-85748 Garching, Germany*

(Dated: July 8, 2014)

We study two-cluster solutions of an ensemble of generic limit-cycle oscillators in the vicinity of a Hopf bifurcation, i.e. Stuart-Landau oscillators, with a nonlinear global coupling. This coupling leads to conserved mean-field oscillations acting back on the individual oscillators as a forcing. A reduction to two effective equations makes a linear stability analysis of the cluster solutions possible. These equations exhibit a π-rotational symmetry, leading to a complex bifurcation structure and a wide variety of solutions. In fact, the principal bifurcation structure resembles that of a 2:1 resonance tongue, while inside the tongue we observe an 1:1 entrainment.

arXiv:1407.1711v1 [nlin.CD] 7 Jul 2014

I. INTRODUCTION

Cluster formation is a well known phenomenon in systems of coupled oscillators. It arises in discrete systems of individual units [1–3] and in spatially extended oscillatory media [4–8]. The common property of clusters in these systems is that the oscillators separate into distinct groups having the same properties within. The oscillations in the different groups are then phase shifted with respect to each other. In the symmetrical phase cluster state, the phase shifts for n clusters are given by $2\pi m/n$ [2, 7, 8], where $m = 1, 2, \ldots, n-1$. Here, we will treat two-cluster solutions, exhibiting more complex than simple periodic dynamics. In many cases the amplitude variations in these states are very small and the dynamics can be approximated by phase models. However, as one prominent counter example, we present a type of clusters, so-called type II clusters [9], where essential variations in the amplitudes occur. They have been described in Refs. [9–12]. In this state the clusters are a modulation of a homogeneous oscillation, as visible in Fig. 1a.

The photoelectrodissolution of n-type silicon [10, 13] is an experimental system exhibiting this type of clustering. Many of the spatio-temporal dynamics of this system can be modelled with a complex Ginzburg-Landau equation (CGLE) with a nonlinear global coupling [11, 14]. As the essential ingredient for the dynamics is this nonlinear global coupling [15], we drop the diffusive coupling of the CGLE, rendering a mathematical treatment of the cluster solutions possible. Thus, in this Article we are dealing with an ensemble of Stuart-Landau oscillators, coupled via a nonlinear global coupling. As we will see, this coupling leads to a conserved periodic mean-field oscillation that acts back on the individual oscillators as a forcing. Then, we reduce the full set of equations to two effective equations describing the case of clustering with two groups. We show that we end up with an equation possessing the same (symmetry) properties as the resonantly forced CGLE near a 2:1 resonance, which also exhibits cluster formation. The symmetry of this equation leads to a very complex bifurcation diagram and therefore to a wide variety of different dynamical states, in line with results on periodically forced oscillators near a 2:1 resonance [16, 17], with one exception: inside the locking region we observe an 1:1 entrainment, despite the bifurcation structure of a 2:1 resonance.

II. STUART-LANDAU OSCILLATORS WITH A CONSERVATION LAW

Our model consists of N Stuart-Landau oscillators, each of the form [3, 18, 19]

$$\frac{\mathrm{d}}{\mathrm{d}t}W_k = W_k - (1+ic_2)\,|W_k|^2\,W_k\ , \quad k = 1, \ldots, N\ , \tag{1}$$

coupled via a nonlinear global coupling [10, 14]:

$$\begin{aligned}\frac{\mathrm{d}}{\mathrm{d}t}W_k =& W_k - (1+ic_2)\,|W_k|^2\,W_k \\ &- (1+i\nu)\,\langle W\rangle + (1+ic_2)\left\langle |W|^2\,W\right\rangle\ .\end{aligned} \tag{2}$$

Here $\langle \ldots \rangle$ describes the arithmetic mean over the oscillator population, i.e. $\langle W\rangle = \sum_{k=1}^{N} W_k/N$. Taking the average of the whole equation yields for the dynamics of the mean value

$$\frac{\mathrm{d}}{\mathrm{d}t}\langle W\rangle = -i\nu\,\langle W\rangle \quad \Rightarrow \quad \langle W\rangle = \eta e^{-i\nu t}\ . \tag{3}$$

Therefore, we are dealing with a globally coupled population of Stuart-Landau oscillators with a conservation law for the mean-field oscillation. This conservation is an important property of the dynamics of the experimental

* krischer@ph.tum.de

silicon system. Here, we achieve it by the specific design of our coupling function. This mean-field oscillation also acts as an intrinsic self-forcing on the individual oscillators. We will see that this indeed leads to a so-called Arnold tongue, a tongue-shaped region in which the oscillations are entrained to the driving. In general, the dynamics of the oscillator population, Eqs. (2), is determined by three parameters, namely c_2, ν and η.

Equations (2) are equivariant to the direct product $\mathbf{S}_N \times S^1$ of the symmetry group $\mathbf{S}_N$ of permutations of N elements and the circle group S^1, describing the global phase invariance. The equivariance to $\mathbf{S}_N$ is obvious, as a permutation of the indices in Eqs. (2) leaves the whole set of equations invariant. Nevertheless, particular solutions are not required to possess the full $\mathbf{S}_N \times S^1$ symmetry, only all solutions together exhibit it [20].

We numerically solved Eqs. (2) using an implicit Adams method with timestep $dt = 0.01$. For certain parameter regimes the whole population divides into two subgroups of size N_1 and N_2 with $N_1 + N_2 = N$. Thus, the full symmetry is reduced to $\mathbf{S}_{N_1} \times \mathbf{S}_{N_2} \times S^1 \subseteq \mathbf{S}_N \times S^1$. For $\eta > 0$ one then observes modulated amplitude and amplitude clusters as shown in Figs. 1a and b, respectively.

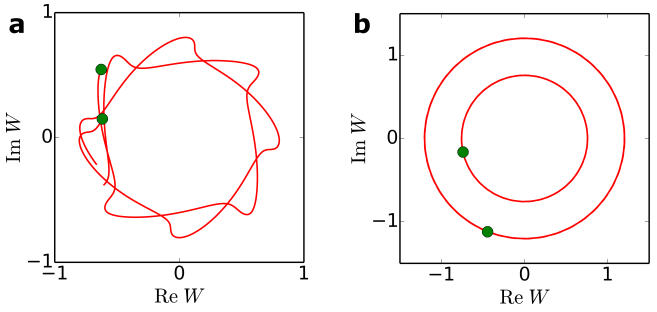

FIG. 1. Cluster dynamics in the Stuart-Landau ensemble. Lines describe the trajectories and dots mark the positions in a snapshot. (a) Modulated amplitude clusters for $c_2 = -0.6$, $\nu = 0.1$ and $\eta = 0.7$. Here, the subgroups perform additional oscillations around their mean-field $\eta \exp(-i\nu t)$ given in Eq. (3). (b) Amplitude clusters for $c_2 = -0.6$, $\nu = -1.5$ and $\eta = 0.9$. The main differences between the two groups are the different radii of their respective limit cycles. The phase shift is much smaller than π.

In the modulated amplitude cluster state the subgroups oscillate, in addition to the mean-field oscillation, around their mean field. This leads to a repeated passing by each other of the subgroups in the complex plane. Similar states were observed in continuous systems in Refs. [5, 9–12, 21]. In the amplitude cluster state the two groups oscillate on different limit cycles separated by an amplitude difference, while the phase shift is much smaller than π [19]. In the next section, in order to treat these solutions mathematically, we reduce the full set of N equations in Eqs. (2) to two effective equations modelling the two subgroups.

III. MODULATED AMPLITUDE CLUSTERS IN THE TWO-GROUPS REDUCTION

We will now focus on the modulated amplitude clusters as presented in Fig. 1a. As visible from the figure, the ensemble splits into two groups, each performing amplitude-modulated oscillations in the complex plane. To analyze these dynamics, we reduce the N equations of the Stuart-Landau ensemble, Eqs. (2), to two effective equations. Therefore, we assume two groups W_1 and W_2, each synchronized, with sizes N_1 and N_2, respectively. The average over the entire ensemble is then given by

$$\langle W \rangle = \frac{1}{N} \left(N_1 W_1 + N_2 W_2 \right) \ , \tag{4}$$

and analogously for $\left\langle |W|^2 W \right\rangle$. Inserting these expressions into Eqs. (2) results in

$$\begin{aligned} \frac{\mathrm{d}}{\mathrm{d}t} W_1 = & \left(1 - (1 + i\nu) \frac{N_1}{N} \right) W_1 \\ & - (1 + ic_2) \left(1 - \frac{N_1}{N} \right) |W_1|^2 W_1 \\ & - (1 + i\nu) \frac{N_2}{N} W_2 + (1 + ic_2) \frac{N_2}{N} |W_2|^2 W_2 \ , \end{aligned} \tag{5}$$

where the same holds for W_2 with indices 1 and 2 interchanged. Thus, we reduced the set of N equations to two effective equations and can now perform a linear stability analysis of the synchronized state. By setting $W_1 = W_2$ we obtain

$$\frac{\mathrm{d}}{\mathrm{d}t} W_1 = \frac{\mathrm{d}}{\mathrm{d}t} W_2 = -i\nu W_1 = -i\nu W_2 \ , \tag{6}$$

and thus

$$W_1 = W_2 = \eta e^{-i\nu t} = W_0 \ , \tag{7}$$

as expected. Since the conservation law, Eq. (3), still has to be fulfilled, the synchronized solution is given by W_0. We define deviations w_1 and w_2 from W_0 via $W_1 = W_0(1 + w_1)$ and $W_2 = W_0(1 + w_2)$. To fulfill the conservation law,

$$\frac{1}{N} \left(N_1 w_1 + N_2 w_2 \right) = 0 \tag{8}$$

holds. For symmetric cluster states $N_1 = N_2 = N/2$ one obtains for w_1 and w_2, when using the condition in Eq. (8),

$$\begin{aligned} \frac{\mathrm{d}}{\mathrm{d}t} w_1 &= (\mu + i\beta)\, w_1 - (1 + ic_2)\eta^2 \left(|w_1|^2 w_1 + w_1^* \right) \ , \\ w_2 &= -w_1 \ , \end{aligned} \tag{9}$$

where $\mu = 1 - 2\eta^2$ and $\beta = \nu - 2\eta^2 c_2$.

Note here already that the equation for w_1 is a forced CGLE near a 2:1 resonance [22] without the diffusive coupling, which is a result of the self-forcing in the system. The synchronized solution W_0 possesses the symmetry $\mathbf{S}_2 \times S^1$ in the present two-oscillators description. A bifurcation with emanating solution branches exhibiting the reduced symmetry S^1 (separation into two subgroups) has to have the following symmetry property: the sum of the two solutions $W_1 + W_2$ is required to possess the full symmetry $\mathbf{S}_2 \times S^1$ (W_1 is on one of the solution branches and W_2 on another). Therefore, the symmetry breaking parts w_1 and w_2 have to cancel each other, i.e. $w_1 = -w_2$. This symmetry condition is fulfilled by three types of bifurcations, namely the pitchfork, the Hopf and the period doubling bifurcations. In case of the Hopf and the period doubling bifurcations the two solution branches are phase shifted by π. We will see that we indeed find the pitchfork and the Hopf bifurcation in the following linear stability analysis of the synchronized state, which is given by $w_1 = w_2 = 0$. The linear stability of this state is determined by

$$\frac{\mathrm{d}}{\mathrm{d}t}\begin{pmatrix} w_1 \\ w_1^* \end{pmatrix} = \begin{pmatrix} \mu + i\beta & -(1+ic_2)\eta^2 \\ -(1-ic_2)\eta^2 & \mu - i\beta \end{pmatrix} \cdot \begin{pmatrix} w_1 \\ w_1^* \end{pmatrix} . \tag{10}$$

The eigenvalues of the Jacobian matrix are given by

$$\lambda_\pm = 1 - 2\eta^2 \pm \sqrt{\eta^4\left(1 - 3c_2^2\right) + 4\nu c_2 \eta^2 - \nu^2} . \tag{11}$$

Thus, we find a secondary Hopf bifurcation in this system at $\eta = \eta_H = 1/\sqrt{2}$ for $\left(1 - 3c_2^2\right)/4 + 2\nu c_2 - \nu^2 < 0$. This Hopf bifurcation is the origin of the modulated amplitude clusters shown in Fig. 1a. In order to visualize this, we use the ansatz $W_k = W_0(1 + w_k)$ in the full system (Eqs. (2)) for the analysis of simulation results. An example for the dynamics of w_k in case of the modulated amplitude cluster state is shown in Fig. 2a.

One can clearly identify the two limit cycles of the two subgroups (blue solid lines). The green dots mark a snapshot of the dynamics. In this reference frame the phase shift between the two groups is given by π. The two limit cycles are not identical, since the full system is divided into two groups with different sizes, i.e. $N_1 \neq N_2$. This results in different radii of the limit cycles in order to fulfill the condition in Eq. (8) and thus to fulfill the conservation law in Eq. (3). The red square marks the position of the synchronized solution. These observations confirm the result of the two-groups analysis that the modulated amplitude clusters arise in a secondary Hopf bifurcation. Transforming the system back to W_k, one obtains the dynamics shown in Fig. 2b.

Using the eigenvalues in Eq. (11) we can determine the Hopf frequency ω_H to be

$$\omega_H = \mathrm{Im}\left(\sqrt{\eta^4\left(1 - 3c_2^2\right) + 4c_2\eta^2\nu - \nu^2}\right) . \tag{12}$$

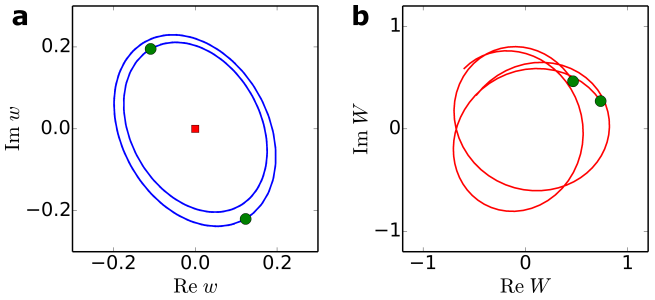

FIG. 2. Emergence of modulated amplitude clusters in the full ensemble for $c_2 = -0.6$, $\nu = 1.2$ and $\eta = 0.7$. (a) Two limit cycles in anti phase and the fixed point at η (red square) in the rotating frame of w_k defined via $W_k = W_0(1 + w_k)$. The limit cycles have different radii as the whole population is divided into subgroups with $N_1 \neq N_2$. (b) Dynamics in the original system.

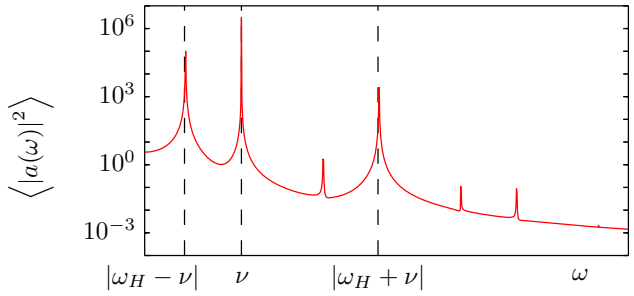

FIG. 3. Cumulative power spectrum for the full system at parameter values $c_2 = -0.6$, $\nu = 1.2$, $\eta = 0.7$. The major peaks in this spectrum can be traced back to linear combinations of the Hopf frequency ω_H in Eq. (12) and the frequency of the mean-field oscillation ν as indicated by the vertical lines (see text and Eq. (15)).

Next, we investigate the frequencies occurring in the dynamics in the original frame. Therefore, we calculate the cumulative power spectrum. To obtain this, one first has to Fourier transform all individual time series Re W_k of the oscillators and then average the resulting squared amplitudes $|a_k(\omega)|^2$, where k is the oscillator index. It is thus given by $S(\omega) = \left\langle |a(\omega)|^2 \right\rangle$. An exemplary cumulative power spectrum for the dynamics in the modulated amplitude cluster state (in the full system) is shown in Fig. 3 and it exhibits several peaks.

The strongest peak is at the frequency ν of the average-oscillation. As we will show in what follows, the next two highest peaks are given by $\pm(\nu - \omega_H)$ and $\pm(\nu + \omega_H)$ as indicated by vertical lines in the figure.

In the vicinity of the Hopf bifurcation, the limit-cycle solution for w_1 in Eq. (9) is given by

$$w_1 = w_+^0 e^{i\omega_H t} + w_-^0 e^{-i\omega_H t} , \tag{13}$$

where $w_\pm^0$ are complex-valued constants. In the origi-

nal frame this results in

$$W_1 = \eta e^{-i\nu t}\left(1 + w_+^0 e^{i\omega_H t} + w_-^0 e^{-i\omega_H t}\right) ,$$
$$W_2 = \eta e^{-i\nu t}\left(1 - w_+^0 e^{i\omega_H t} - w_-^0 e^{-i\omega_H t}\right) . \qquad (14)$$

Thus, we obtain frequency contributions in the cumulative power spectrum at

$$\begin{aligned} &\pm\nu \quad \left(\propto \eta^2\right) , \\ &\pm(\nu - \omega_H) \quad \left(\propto \left(\eta\omega_+^0\right)^2\right) , \\ &\pm(\nu + \omega_H) \quad \left(\propto \left(\eta\omega_-^0\right)^2\right) , \end{aligned} \qquad (15)$$

as can be seen for the three major peaks in the power spectrum in Fig. 3. The other peaks are presumably given by higher resonances. Note that for a circular limit cycle ω_+^0 or ω_-^0 equals zero leading to vanishing contributions at $\pm(\nu - \omega_H)$ or $\pm(\nu + \omega_H)$, respectively.

To further check the validity of the frequencies, obtained via a reduction to two effective equations and via linear stability analysis, we compare them with the frequencies in the full system for several values of ν. The results for $|\nu + \omega_H|$ (blue, dashed) and $|\nu - \omega_H|$ (red, solid) are shown in Fig. 4a. In Fig. 4b we show the comparison for $|\nu - \omega_H|$ in more detail.

The simulation results shown are for $\eta = 0.7$, which is close to the value at the Hopf bifurcation $\eta_H = 1/\sqrt{2} \approx 0.707$. As visible in the figure, the results of the linear stability analysis (lines), Eq. (15), reproduce the simulation results (symbols) very well. The nearly constant shift visible in Fig. 4b is due to the finite distance to the Hopf bifurcation.

We conclude that the modulated amplitude clusters arise through a Hopf bifurcation in the rotating frame with frequency ν, which gives rise to the amplitude modulations in the full system. The dynamics on the created limit cycle are in anti-phase as to fulfill the conservation law, which is also in line with our symmetry considerations above. Since the Hopf bifurcation occurs in the rotating frame, it is in fact a secondary Hopf bifurcation. The dynamics in the original frame is thus quasiperiodic. This is also obvious from the continuous frequency curves in Fig. 4.

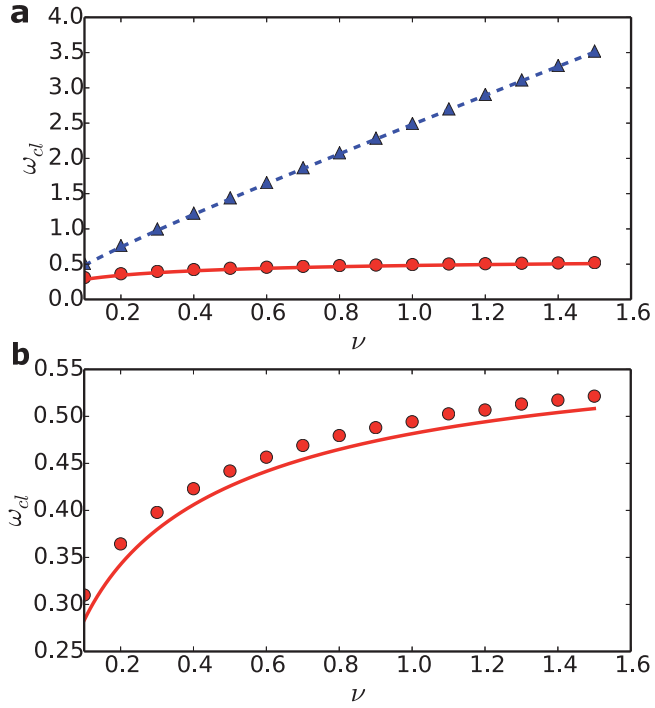

FIG. 4. Comparison of the calculated peak frequencies with the frequencies in the full system for $c_2 = -0.6$ and $\eta = 0.7$. The Hopf bifurcation occurs at $\eta_H = 1/\sqrt{2}$. (a) Both frequencies $|\nu + \omega_H|$ in blue (dashed) and $|\nu - \omega_H|$ in red (solid) versus ν. Lines describe the results of the linear stability analysis, Eq. (15), and symbols mark the simulation results. (b) For more details only $|\nu - \omega_H|$ vs. ν.

IV. AMPLITUDE CLUSTERS IN THE TWO-GROUPS REDUCTION

The modulated amplitude clusters described in the preceding section arise for certain parameters through a Hopf bifurcation. This motion on a torus can be destroyed through a saddle-node bifurcation leading to the amplitude clusters shown in Fig. 1b. These amplitude clusters are solutions of Eq. (9) in the form $w_1 = R\exp(i\chi_\pm)$ [22], as this results in $|W_1| = \eta\sqrt{1 + 2R\cos\chi_\pm + R^2}$. With $\chi_+ = \chi_- + \pi$ the two solutions describe limit cycles with different radii. Inserting this ansatz into Eq. (9), separating real and imaginary parts and assuming $R \neq 0$ one obtains

$$\mu - \eta^2 R^2 - \eta^2\cos 2\chi - c_2\eta^2\sin 2\chi = 0 ,$$
$$\beta - c_2\eta^2 R^2 - c_2\eta^2\cos 2\chi + \eta^2\sin 2\chi = 0 . \qquad (16)$$

This set of equations can be solved for R and χ and one finds two pairs of solutions [23, 24]:

$$
\begin{aligned}
R^{(1)} &= \sqrt{\frac{\mu + c_2\beta - \sqrt{\eta^4\left(1+c_2^2\right)^2 - (c_2-\nu)^2}}{\eta^2\left(1+c_2^2\right)}}\ , \\
\chi_-^{(1)} &= \frac{1}{2}\arcsin\left(\frac{c_2-\nu}{\eta^2\left(1+c_2^2\right)}\right)\ , \\
\chi_+^{(1)} &= \chi_-^{(1)} + \pi\ ,
\end{aligned}
\tag{17}
$$

$$
\begin{aligned}
R^{(2)} &= \sqrt{\frac{\mu + c_2\beta + \sqrt{\eta^4\left(1+c_2^2\right)^2 - (c_2-\nu)^2}}{\eta^2\left(1+c_2^2\right)}}\ , \\
\chi_-^{(2)} &= \frac{\pi}{2} - \frac{1}{2}\arcsin\left(\frac{c_2-\nu}{\eta^2\left(1+c_2^2\right)}\right)\ , \\
\chi_+^{(2)} &= \chi_-^{(2)} + \pi\ .
\end{aligned}
\tag{18}
$$

We calculate the boundaries $\eta(c_2,\nu)$ of their existence and obtain:

$$
R^{(1)},\ \chi_\pm^{(1)} \text{ exists for } \eta > \eta_{SN} \wedge \eta < \eta_c \wedge \eta < \eta_P^-\ , \tag{19}
$$

$$
R^{(2)},\ \chi_\pm^{(2)} \text{ exists for } \begin{cases} \eta > \eta_{SN}\ , & \text{for } \eta < \eta_c\ , \\ \eta_P^- < \eta < \eta_P^+\ , & \text{for } \eta > \eta_c\ . \end{cases} \tag{20}
$$

$\eta_{SN}(c_2,\nu)$, $\eta_c(c_2,\nu)$ and $\eta_P^\pm(c_2,\nu)$ are given by

$$
\begin{aligned}
\eta_{SN} &= \sqrt{\frac{|c_2-\nu|}{1+c_2^2}}\ , \\
\eta_c &= \sqrt{\frac{1+c_2\nu}{2\left(1+c_2^2\right)}}\ , \\
\eta_P^\pm &= \sqrt{\frac{2(1+c_2\nu) \pm \sqrt{4(1+c_2\nu)^2 - 3\left(1+c_2^2\right)\left(1+\nu^2\right)}}{3\left(1+c_2^2\right)}}\ .
\end{aligned}
\tag{21}
$$

Linear stability analysis reveals that the amplitude cluster solutions $R^{(1,2)}\exp\left(i\chi_\pm^{(1,2)}\right)$ arise as two saddle-node pairs at η_{SN}, thereby destroying the limit cycle of the modulated amplitude clusters in a saddle-node of infinite period bifurcation (sniper). Solution (1) is a saddle and solution (2) is a stable node. Both solutions (1) and (2) can be destroyed in a pitchfork bifurcation with the synchronized solution. For details see the next section. In essence, the amplitude clusters emerge in a sniper bifurcation when coming from a parameter region, where the modulated amplitude clusters are stable. And they arise in a pitchfork bifurcation when coming from a parameter region, where the synchronized solution is stable (in a small region they also arise via a saddle-node bifurcation; see next section). A coarse bifurcation diagram is depicted in Fig. 5 with illustrations of the dynamical states along the path A to E given in Fig. 6.

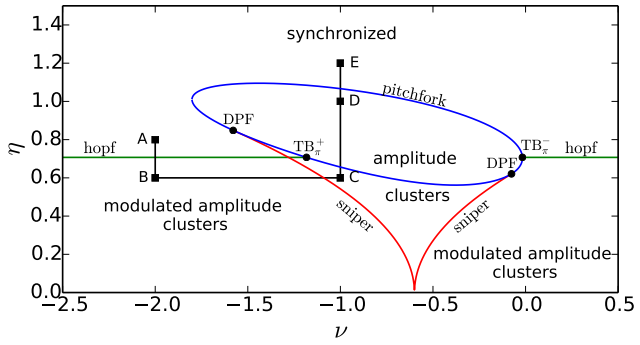

FIG. 5. Coarse bifurcation diagram for the two-groups reduction. Shown is the parameter space η vs. ν for fixed $c_2 = -0.6$. The stable dynamical states are indicated in the figure. The Hopf bifurcation (green) is given by $\eta = \eta_H$, the pitchfork (blue) is described by $\eta_P^\pm$ and the sniper (red) occurs at η_{SN}, see Eqs. (21). The dynamical states along the path A to E are depicted in Fig. 6. The codimension-two points are two Takens-Bogdanov points of π-rotational symmetry (TB$_\pi^\pm$) and two degenerate pitchfork bifurcations (DPF). The details of the bifurcation structure, which have been omitted here, including the unfoldings of the TB$_\pi^\pm$ points, will be discussed in Section V.

The overall structure reminds of a so-called Arnold tongue and we will discuss the relation to the locking behaviour of forced oscillatory media in Section VI. Inside the tongue one observes amplitude clusters. The tongue is bounded by a sniper bifurcation for small η values and by a pitchfork bifurcation for high η values. A hopf bifurcation separates the region of modulated amplitude clusters from the region of stable synchronized solutions. To illustrate the different dynamical behaviors in the distinct regions, we go through the path A to E (for comparison see Fig. 6): Starting at A with the synchronized solution, the hopf bifurcation creates the limit cycle for the modulated amplitude clusters in B. This limit cycle is then destroyed by the sniper bifurcation resulting in amplitude clusters in C. Approaching the outer pitchfork bifurcation brings the fixed points of the amplitude clusters closer together in D. At the pitchfork the fixed points of the amplitude clusters merge with the synchronized solution with what we end up in E. Note that, as $w_2 = -w_1$ in Eq. (9), both groups undergo the bifurcations simultaneously and the second group always realizes the π-rotated solution of the first group.

Furthermore we encounter three codimension-two bifurcations, namely a degenerate pitchfork (DPF) and two types of Takens-Bogdanov points TB$_\pi^\pm$. The unfoldings of the Takens-Bogdanov points are presented in the next Section. Note that due to the symmetry present in the system, the unfoldings are much more complicated than in the standard case.

This diagram is strictly valid only for the two-groups reduction. It clarifies, which bifurcations lead to the amplitude and modulated amplitude clusters. The diagram is applicable whenever the full ensemble is separated into

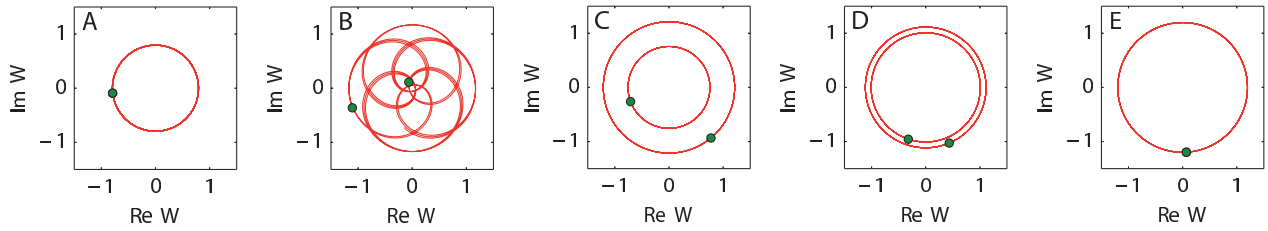

FIG. 6. Simulation results for the two-groups reduction in the original frame illustrating the dynamical states along the path A-E in the bifurcation diagram in Fig. 5.

two subgroups.

V. DETAILS OF THE BIFURCATION DIAGRAM

The codimension-two bifurcations $TB_\pi^\pm$ present in the coarse bifurcation diagram in Fig. 5 have rather complex unfoldings. Using the software `AUTO-07P` for numerical continuation, we could identify the local and global bifurcations occurring around the $TB_\pi^\pm$ points. The unfolding of the plus case, TB_π^+, is shown schematically in Fig. 7, while the minus case, TB_π^-, is presented in Fig. 8. Sketches of corresponding phase portraits are also depicted in the figures.

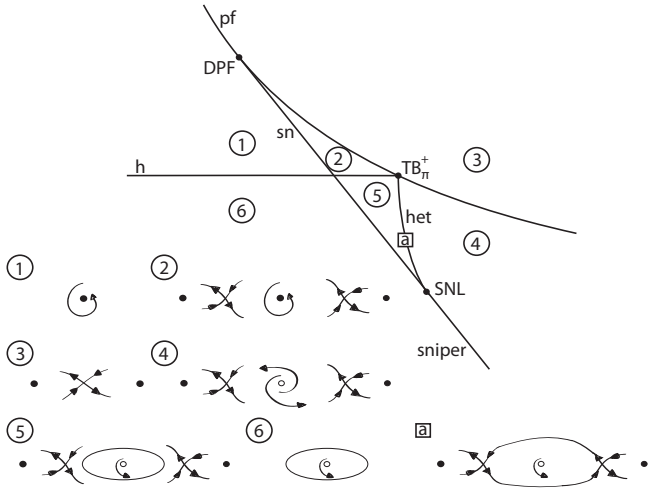

FIG. 7. Sketch of the local bifurcation structure around the TB_π^+ point with corresponding phase portraits. The involved codimension-one bifurcations are: pitchfork (pf), saddle-node (sn), Hopf (h), saddle-node of infinite period (sniper) and heteroclinic (het). The codimension-two bifurcations are: Takens-Bogdanov TB_π^+, degenerate pitchfork (DPF) and saddle-node loop (SNL). Stable fixed points are marked by filled circles and unstable ones by empty circles. Stable limit cycles are drawn with a solid line and unstable limit cycles with a dashed line.

In the TB_π^+ point a pitchfork, a Hopf and a heteroclinic bifurcation meet. In our system, we find in the vicinity

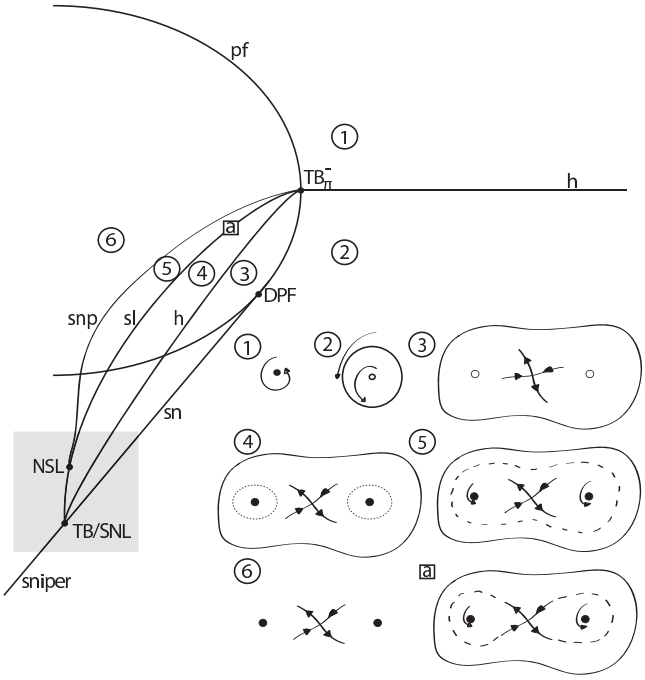

FIG. 8. Sketch of the local bifurcation structure around the TB_π^- point with corresponding phase portraits. The involved codimension-one bifurcations are: pitchfork (pf), saddle-node (sn), Hopf (h), saddle-node of infinite period (sniper), saddle-loop (sl) and saddle-node of periodic orbits (snp). The codimension-two bifurcations are: Takens-Bogdanov with symmetry (TB_π^-) and without symmetry (TB), saddle-node loop (SNL), degenerate pitchfork (DPF) and neutral saddle-loop (NSL). Here, a TB and a SNL belonging to different solutions coincide, for details see text. Stable fixed points are marked by filled circles and unstable ones by empty circles. Stable limit cycles are drawn with a solid line and unstable limit cycles with a dashed line. Note that the bifurcation structure in the shaded box is not a result of the continuation as this diverges. It is consistent with the rest of the diagram, but there might be other bifurcations involved, see e.g. Ref. [16].

also a saddle-node bifurcation, which meets the pitchfork in a degenerate pitchfork bifurcation (DPF) and the heteroclinic in a saddle-node loop (SNL) bifurcation, see Fig. 7. The DPF turns the pitchfork from supercritical to subcritical and the TB_π^+ changes it back to supercrit-

ical. The SNL turns the saddle-node into a saddle-node of infinite period (sniper).

When following the numbering in Fig. 7, we start with a stable focus (1), then cross the saddle-node, thereby creating two saddle node pairs (2). Then, we cross the subcritical pitchfork and end up in (3) with two stable nodes and a saddle. Next, we cross the pitchfork on the supercritical side, yielding two saddle node pairs with an unstable focus in between (4). Note that the foci involved in the pitchfork bifurcations change to nodes just before the bifurcations occur. Crossing the heteroclinic bifurcation creates a stable limit cycle around the unstable focus in the center (5), which emerges from a double heteroclinic connection at the bifurcation (a). Finally, the saddle node pairs are annihilated in a saddle-node bifurcation and we are left with a stable limit cycle around an unstable focus in (6).

The local bifurcation structure around the TB_π^- point is more complex. In the TB_π^- point, a pitchfork, a Hopf concerning the synchronized solution, a Hopf concerning the amplitude cluster solutions, a saddle-loop and a saddle-node of periodic orbits (snp) meet. The saddle-loop line is in fact the coincidence of two saddle-loop bifurcations, one which describes the saddle-loop bifurcation of the amplitude cluster solutions (small limit cycles in Fig. 8) and one which concerns the modulated amplitude cluster solutions (outer limit cycles in Fig. 8). With this, we can understand the codimension-two bifurcations occurring in the vicinity of the TB_π^- point: the snp and the two saddle-loops meet first in a neutral saddle-loop (NSL) and later the saddle-loops meet with the hopf and the saddle-node in a Takens-Bogdanov (TB) without symmetry and a saddle-node loop (SNL). The saddle-loop corresponding to the amplitude cluster solution ends in the TB point and the other saddle-loop turns the saddle-node into a saddle-node of infinite period (sniper) at the SNL. Note that this region of the bifurcation diagram, i.e. the shaded region, is not a result of the continuation as this diverges. It is consistent with the rest of the diagram, but there might be other bifurcations involved, see e.g. Ref. [16]. In the degenerate pitchfork (DPF) the saddle-node bifurcation meets the pitchfork.

Again we can go through the diagram step by step by following the numbering in Fig. 8: We start with a stable focus (1) and cross the Hopf to obtain a stable limit cycle around an unstable focus (2). Then, the subcritical pitchfork turns the unstable focus into a saddle point and creates two unstable nodes (3). The subcritical hopf creates two unstable limit cycles (4), which form homoclinic loops when meeting the manifolds of the saddle point in the saddle-loop bifurcation (a). This saddle-loop bifurcation coincides with a saddle-loop bifurcation of an unstable modulated amplitude cluster solution, which is given by the unstable limit cycle in (5). Finally, the stable and the unstable limit cycle annihilate each other in a snp, and a pair of stable nodes (describing the amplitude cluster solutions) with a saddle point in between remain (6).

In fact the $\mathrm{TB}_\pi^\pm$ points are Takens-Bogdanov points of π-rotational or cubic symmetry [25, 26]. This is the symmetry present in Eq. (9). They possess the same principal bifurcation structure as the second order resonance points found in the investigation of periodically forced oscillators [16]. However, some bifurcations are different, as we will discuss in the next section.

VI. CONCLUSIONS

We could unravel the complex bifurcation structure exhibited by the two-cluster solutions of an ensemble of generic limit-cycle oscillators near a Hopf bifurcation. The conservation of the mean-field oscillations leads to mainly two bifurcations: a Hopf bifurcation yielding the modulated amplitude clusters and a pitchfork bifurcation resulting in common amplitude clusters. The meeting of these two gives rise to two Takens-Bogdanov points of π-rotational symmetry and therewith to a wide variety of dynamical states.

Besides the application to the experimental system, for which the model was originally proposed, namely the photoelectrodissolution of n-type silicon [10, 11, 13], there is a strong connection to resonantly forced oscillatory media [7, 8, 22, 27–33]. The symmetry properties of the reduced dynamics in Eq. (9), namely the cubic and π-rotational symmetries, are also present in the complex Ginzburg-Landau equation (CGLE) with resonant forcing near a 2:1 resonance. In fact, there is a linear transformation that transforms the equation for w_1 in Eq. (9) to the form given in e.g. Ref. [22] (see Eq. (10) therein) of the resonantly forced CGLE, when omitting the diffusive coupling. As for forced oscillatory media, we observe an Arnold tongue, a region of frequency locking, in the bifurcation diagram in Fig. 5. The tongue starts at $\nu = c_2$, i.e. at a value of the driving frequency ν equal to the natural frequency of the Stuart-Landau oscillator c_2. The locking region is bounded by the saddle-node, sniper and pitchfork bifurcations. The dynamics lock to the frequency ν of the mean-field oscillations, i.e. to the frequency of the driving. Thus, we observe an 1:1 locking instead of a 2:1 locking, which one would expect, since we observe the bifurcation structure of a 2:1 resonance. This is reflected in the occurrence of a pitchfork bifurcation instead of the period doubling bifurcation, see Ref. [16]. Furthermore, as in the forced CGLE, the locked solutions do not lie on a torus, since the torus is destroyed in a sniper bifurcation.

In our system the forcing is in fact a self-forcing, as the dynamics produce a mean-field oscillation, which is conserved and then acts back as a forcing on the system. This self-forcing renders the cluster solutions possible. But note that it is the mathematical structure of a 2:1 resonance that is responsible for the cluster formation. We observe an 1:1 locking and in general this would not give rise to cluster formation.

ACKNOWLEDGMENTS

We thank Vladimir García-Morales for fruitful discussions, his comments on the symmetry considerations and for careful reading of the manuscript. The authors gratefully acknowledge financial support from the *Deutsche Forschungsgemeinschaft* (Grant no. KR1189/12-1), the *Institute for Advanced Study, Technische Universität München* funded by the German Excellence Initiative and the cluster of excellence *Nanosystems Initiative Munich (NIM)*.

[1] K. Kaneko, Physica D: Nonlinear Phenomena **41**, 137 (1990).
[2] K. Okuda, Physica D: Nonlinear Phenomena **63**, 424 (1993).
[3] N. Nakagawa and Y. Kuramoto, Physica D: Nonlinear Phenomena **75**, 74 (1994).
[4] V. K. Vanag, L. Yang, M. Dolnik, A. M. Zhabotinsky, and I. R. Epstein, Nature **406**, 389 (2000).
[5] V. K. Vanag, A. M. Zhabotinsky, and I. R. Epstein, J. Phys. Chem. A **104**, 11566 (2000).
[6] A. S. Mikhailov and K. Showalter, Physics Reports **425**, 79 (2006).
[7] A. L. Lin, A. Hagberg, E. Meron, and H. L. Swinney, Phys. Rev. E **69**, 066217 (2004).
[8] P. Kaira, P. S. Bodega, C. Punckt, H. H. Rotermund, and D. Krefting, Phys. Rev. E **77**, 046106 (2008).
[9] H. Varela, C. Beta, A. Bonnefont, and K. Krischer, Phys. Chem. Chem. Phys. **7**, 2429 (2005).
[10] I. Miethe, V. García-Morales, and K. Krischer, Phys. Rev. Lett. **102**, 194101 (2009).
[11] V. García-Morales, A. Orlov, and K. Krischer, Phys. Rev. E **82**, 065202 (2010).
[12] M. Bertram, C. Beta, H. H. Rotermund, and G. Ertl, The Journal of Physical Chemistry B **107**, 9610 (2003), http://pubs.acs.org/doi/pdf/10.1021/jp0341927.
[13] K. Schönleber, C. Zensen, A. Heinrich, and K. Krischer, New Journal of Physics **16**, 063024 (2014).
[14] L. Schmidt, K. Schönleber, K. Krischer, and V. García-Morales, Chaos: An Interdisciplinary Journal of Nonlinear Science **24**, 013102 (2014).
[15] L. Schmidt, K. Schönleber, V. García-Morales, and K. Krischer, arXiv , 1405.0414 (2014).
[16] W. Vance and J. Ross, The Journal of Chemical Physics **91**, 7654 (1989).
[17] W. N. Vance and J. Ross, Chaos: An Interdisciplinary Journal of Nonlinear Science **1**, 445 (1991).
[18] Y. Kuramoto, *Chemical Oscillations, Waves, and Turbulence* (Dover Publications, Inc., Mineola, New York, 2003).
[19] H. Daido and K. Nakanishi, Phys. Rev. Lett. **96**, 054101 (2006).
[20] M. Golubitsky and I. Stewart, *The Symmetry Perspective: From Equilibrium to Chaos in Phase Space and Physical Space* (Birkhäuser Verlag, Basel, 2003).
[21] M. Pollmann, M. Bertram, and H. H. Rotermund, Chem. Phys. Lett. **346**, 123 (2001).
[22] P. Coullet and K. Emilsson, Physica D: Nonlinear Phenomena **61**, 119 (1992).
[23] A. Yochelis, A. Hagberg, E. Meron, A. L. Lin, and H. L. Swinney, SIAM J. Appl. Dyn. Sys. **1**, 236 (2002).
[24] A. Yochelis, PhD Thesis, Ben-Gurion University (2004).
[25] J. Guckenheimer and P. Holmes, *Nonlinear Oscillations, Dynamical Systems, and Bifurcations of Vector Fields* (Springer-Verlag New York, Inc., 1983).
[26] J. Guckenheimer, SIAM J. Math. Anal. **15**, 1 (1984).
[27] J. M. Gambaudo, J. Diff. Eqs. **57**, 172 (1985).
[28] V. Petrov, Q. Ouyang, and H. L. Swinney, Nature **388**, 655 (1997).
[29] V. García-Morales and K. Krischer, Contemporary Physics **53**, 79 (2012).
[30] A. Yochelis, C. Elphick, A. Hagberg, and E. Meron, EPL (Europhysics Letters) **69**, 170 (2005).
[31] J. M. Conway and H. Riecke, Phys. Rev. E **76**, 057202 (2007).
[32] B. Marts, A. Hagberg, E. Meron, and A. L. Lin, Chaos **16**, 037113 (2006).
[33] A. Yochelis, C. Elphick, A. Hagberg, and E. Meron, Physica D: Nonlinear Phenomena **199**, 201 (2004), trends in Pattern Formation: Stability , Control and Fluctuations.